MIJST
MIST International Journal of Science and Technology

Detached Eddy Simulations of a Reaction Control Jet from an Axi-Symmetric Body in a Supersonic Crossflow

Raj Kiran Grandhi[1*], and Arnab Roy[2]

[1]Defence Research and Development Organisation, Hyderabad, India, 500058
[2]Indian Institute of Technology, Kharagpur, India, 721302

emails: [1]rajkirangrandhi.asl@gov.in; and [2]arnab@aero.iitkgp.ac.in

ARTICLE INFO

Article History:

Received: 02nd April 2024
Revised: 15th May 2024
Accepted: 15th May 2024
Published: 30th June 2024

Keywords:

Control jet
Pressure
Effectiveness
DES
Transient interaction

ABSTRACT

The introduction of a control jet into a supersonic cross flow yields a substantial region of separated flow, manifesting in the vicinity of the injection site. This, in turn, alters the distribution of pressure on the primary body, thereby influencing the effectiveness of the injected jet's capacity to produce the desired control forces and moments. In the context of an axi-symmetric parent body, this disruption typically leads to a reduction in effectiveness, owing to the overflow of the shock structures encompassing the parent body. The present study investigates the injection of a reaction control jet into a supersonic crossflow using different Detached Eddy Simulation (DES) techniques. The side jet is injected from an orifice on an axi-symmetric parent body, which is aligned with the crossflow direction. The effects of the side jet on the flow field are analysed in terms of general flow features and spectral behaviour of pressure and turbulent kinetic energy. The DES results are compared with those obtained from RANS using various turbulence models. The overall effect of a transient interaction pulse is characterized using URANS and two different DES models.

1. INTRODUCTION

In the realm of launch vehicles, the attainment of attitude control relies upon the utilization of Reaction Control Systems (RCS). These systems hold a distinct advantage over aerodynamic control surfaces, as they can be effectively employed even under conditions of low dynamic pressure during flight, without incurring any detrimental increase in drag when inactive. Within an RCS, the propulsive force is generated through the expulsion of high-pressure gas jets via nozzles positioned at the periphery of the flight vehicle. However, the introduction of the jet instigates a noteworthy disruption within the flow, resulting from the intricate interaction between the jet and the surrounding external flow encompassing the vehicle.

The aerospace community holds great interest in the interaction between a side jet and a supersonic cross flow, as it directly impacts the effectiveness of the jet in producing control forces within RCS systems (Dickmann & Frank, 2006; Raj & Arnab, 2017; Raj & Arnab, 2019a; Valerio et. al., 2009). This interaction also assumes a crucial role in the realm of scramjet engines, influencing jet penetration, mixing, and combustion (Antonino et. al., 2011; Junya et. al., 2011; Rana, et. al., 2011; Soshi & Sanjiva, 2010; Xiaochuan, et. al., 2015). Additionally, it is responsible for the control forces generated by the nozzle in Secondary Injection Thrust Vector Control (SITVC) systems (Rhea, et. al., 2011). The resulting flow field arising from this complex interaction has been extensively investigated by various research groups, employing a wide range of experimental, theoretical, and computational methodologies

A comprehensive understanding of the fundamental physics underlying the interaction between supersonic jets and cross flows has been developed through a series of early investigations (Krishnan, 2013). Figure 1 offers a schematic representation of the intricate flow structure that arises as a consequence of this interaction, wherein the expanding jet finds itself encapsulated within a barrel shock, effectively acting as a barrier against the incursion of the external flow (Adela, 2000). As a result, a bow shock manifests upstream of the injection site, entwining itself around the injected jet. Furthermore, the boundary layer of the cross-flow experiences separation prior to the injection point, giving rise to the formation of a horse shoe vortex that envelops the jet. This interaction structure stands as an emblematic feature of the flow, bearing distinct topological similarities to the flow

observed over bluff objects, such as a truncated cylinder protruding into a supersonic cross flow.

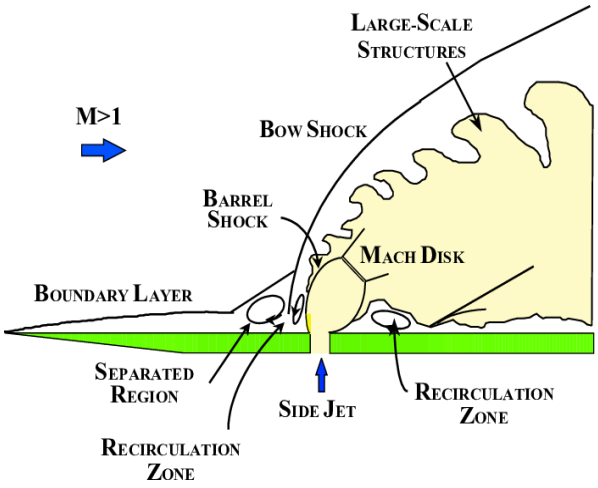

Figure 1: Schematic of the jet interaction flow field [adapted with permission from Adela (2000)]

Extensive research has been devoted to the analysis of injection from an orifice positioned on a flat plate, with significant emphasis placed on studying the phenomena of jet penetration and mixing. In such investigations, injectants such as hydrogen or lighter gases like helium are commonly utilized. The cross-flow Mach number typically lies in the vicinity of 2, although higher Mach numbers are not infrequent. Additionally, the influence of the shape of the injector orifice on the characteristics of the interaction flow field has been explored in various other studies, providing valuable insights into this intricate phenomenon (Sadatake, et. al., 2000). These studies employed a range of computational approaches involving Reynolds Averaged Navier Stokes (RANS) simulations (Adrian, et. al., 2013), scale-resolving simulations such as Large-Eddy Simulations (LES) (Andre, et. al., 2017; Warrick, et. al., 2018) and the hybrid RANS+LES simulations, commonly referred to as Detached- Eddy Simulations (DES) (John, et. al., 2010; Ravichandra & Rodney, 2005; Su-Hee, et. al., 2010). DES methods use RANS in the near wall region or when the cell anisotropy is too high for an LES solution and are thus typically much more computationally tractable than a pure LES simulation.

Soshi and Sanjiva (2010) carried out LES to study the physics of mixing in a scramjet combustor. In order to reduce computational cost, they have carried out the simulation at a Reynolds number based on nozzle diameter of 2.4×10^4 which was one-sixth of the experimental value. To further reduce the computational requirements, only the core region around the injected jet was resolved for LES. Rana, et. al. (2011) used implicit LES to study the jet penetration and mixing characteristics. While the flow conditions in both these studies were the same, the former study used overset meshes and have coupled a "Supersonic Turbulent Boundary Layer" (STBL) simulation that generates the inflow boundary conditions to the supersonic jet mixing simulation whereas the latter study employed synthetic turbulent inflow generation. It should be noted that for the specific jet interaction flow field wherein a sonic or supersonic side jet is injected into a supersonic cross flow, all the scale resolving simulations we found reported in literature were for the interaction due to injection from a flat plate even for the studies pertaining to reaction control systems. We believe this is because of the prohibitive computational cost involved in carrying out LES for injection from a body of revolution. For the purpose of estimating the interaction force, RANS models have been shown to produce acceptable results for a vastly reduced computational effort.

In previous studies, we have reported on the effect of various parameters on the interaction force, the role of curvature on the jet effectiveness (Raj & Arnab, 2019a), explored means of enhancing the performance of the injected jet (Raj & Arnab, 2019b; Raj & Arnab, 2021) and have studied the transient behaviour of various injection profiles on the aerodynamic response (Raj & Arnab, 2023). In the present study, we evaluate several RANS and hybrid RANS+LES models for the jet interaction problem on axisymmetric parent bodies. In addition to discussing the unsteady effects of a reaction control jet corresponding to steady injection, the overall effect of a transient injection in which the side jet is abruptly initiated / withdrawn is studied using Detached Eddy Simulation techniques. The aerodynamic interaction force predicted by DES is compared to those obtained using various RANS models.

2. METHODOLOGY

A. The Jet Effectiveness

When a reaction control jet operates in the presence of an external flow surrounding the vehicle, the overall force response comprises the combined effects of aerodynamic and reaction forces. In the absence of an injected jet, the aerodynamic force is contingent upon factors such as the body's geometry, its attitude relative to the external flow, and the prevailing free stream conditions. However, with the activation of the control jet, the ensuing interaction flow structure alters the pressure distribution across the vehicle. As a result, the total aerodynamic force encompasses contributions from both the geometry/attitude/free stream factors and the forces induced by the interaction. When considering a reaction control jet, the reaction force can be quantified using the equation 1 as follows,

$$F_{\text{jet}} = \dot{m}_{\text{jet}} V_e + (P_e - P_a) \times A_e \tag{1}$$

In order to assess the jet effectiveness under a given flight condition, which encompasses factors such as geometry, body attitude, external conditions, and injection parameters, two simulations are performed. One simulation includes a side jet, while the other does not. The discrepancy in force observed between these two simulations signifies the actual effect of the jet, taking into account the influence of interaction. The jet effectiveness is defined as the ratio between this force difference and the jet reaction (Eq. 2),

serving as a quantifiable metric to evaluate the efficacy of the jet.

$$\mathrm{E_{jet}} = \frac{\Delta F}{F_{\mathrm{jet}}} \tag{2}$$

If the impact of jet interaction on the additional force is deemed insignificant, the difference in force (ΔF) approximates the force generated by the jet itself (F_{jet}), resulting in a jet effectiveness value that is close to unity. The magnitude of the jet effectiveness depends on the alignment of the jet interaction force with respect to the jet reaction. When the forces are in the same direction, the jet effectiveness surpasses unity, whereas in the opposite direction, it falls below unity. This parameter, defined in a similar manner, has also been referred to as the jet/interaction amplification factor or interaction amplification coefficient (Julius & Jacob, 1996; Mitsura, et. al., 2001).

The ultimate aim of operating an RCS thruster is to generate torque for precise attitude control. The interaction between the flow and the surface results in an additional pitching moment which is of significant importance. Whether this interaction moment proves favorable or not depends on the placement of the RCS thruster. If the thruster is positioned ahead of the center of gravity (CG), it is intended to produce a pitch-down moment. In such cases, the interaction moment would be advantageous if it aligns with the pitch-down direction, whereas it would be unfavorable if it opposes it. On the contrary, for an RCS thruster situated behind the CG towards the rear of the parent vehicle, a pitch-up interaction moment is considered beneficial. In terms of the moment about the injection location, this interaction effect can be visualized as causing a displacement of the said location of injection, thereby creating an effective moment arm, given by Eq. 3:

$$X_i = \frac{M_i}{F_{\mathrm{jet}}} \tag{3}$$

Thus, when X_i is zero, it indicates the absence of any interaction moment. A positive value of X_i signifies the existence of a pitch-up moment generated by the interaction, whereas a negative value of X_i indicates a pitch-down moment generated by the interaction.

B. Solver Numerics

The simulations were performed using CFD++[26], a general-purpose CFD solver based on the finite volume approach. In the specific case of this problem, a density-based solver was employed. This solver allows for the simultaneous solution of the continuity, momentum, and energy equations by formulating the governing equations in the following integral Cartesian form (Eq. 4):

$$\frac{\partial}{\partial t}\int_V \mathbf{Q}dV + \oint [\mathbf{F}+\mathbf{G}]\cdot d\mathbf{A} = \int_V \mathbf{S}dV \tag{4}$$

with **S** corresponding to the source terms and the vectors **Q**, **F** and **G** defined as:

$$\mathbf{Q} = \begin{Bmatrix} E \\ \rho \\ \rho u \\ \rho v \\ \rho w \end{Bmatrix} \tag{5}$$

$$\mathbf{F} = \begin{Bmatrix} (E+p)\mathbf{v} \\ \rho\mathbf{v} \\ \rho\mathbf{v}u + p\hat{i} \\ \rho\mathbf{v}v + p\hat{j} \\ \rho\mathbf{v}w + p\hat{k} \end{Bmatrix} \tag{6}$$

$$\mathbf{G} = \begin{Bmatrix} \mathbf{q} - \tau_{ij}v_j \\ 0 \\ -\tau_{xi} \\ -\tau_{yi} \\ -\tau_{zi} \end{Bmatrix} \tag{7}$$

In these equations, p is pressure of the fluid and E is its total energy. τ is the viscous stress tensor and q is the heat flux. The total energy E is related to the total enthalpy, H (= $h+|v|^2/2$) by the relation: $E = \rho H - p$. The ideal gas equation of state is used to close the system of equations.

A second-order implicit "Dual Time Stepping" method was used to evolve the solution temporally, starting from a steady-state initial solution. In this method, the CFD solver appends a pre-conditioned pseudo time derivative term to the non-linear equations and linearizes the flux and source terms to solve for the flow variables at the next physical time step. The global time step, Δt, is explicitly specified and its size is limited only by the level of desired temporal accuracy. This time step is the same over the entire fluid domain. The local or pseudo time step size, $\Delta\tau$, is determined by the solver using the specified CFL condition and varies over the flow domain. For each of the global (or physical) time advancement, several "inner" iterations are carried out till convergence is achieved for that physical time step. In the present series of DES simulations, this global time step size was chosen to be 0.2μs which corresponds to a CFL number of 0.2 – 0.3 depending on the spatial resolution of the employed computational grid.

The simulation methodology was verified through grid independence studies, which were performed to ensure the robustness of the results. The Grid Convergence Index (GCI) was computed to evaluate the convergence of the solution as the grid was refined (Patrick, 2003). The simulation results were validated using the extensive experimental data of Stahl, et. al (2008) for a typical cone-cylinder-flare configuration as shown in figure 2. The comprehensive verification and validation studies conducted in relation to this research were meticulously documented and published by the authors in a previous publication (Raj & Arnab, 2017) and are only briefly mentioned here.

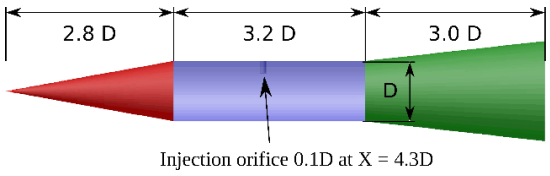

Figure 2: Geometric configuration of Stahl, et. al. (2008)

These studies correspond to steady injection at a total pressure of 3.28MPa and total temperature of 280K into a steady supersonic cross flow with pressure, P_∞ = 16400Pa, temperature, T_∞ = 100K, and Mach number M_∞ = 3.0.

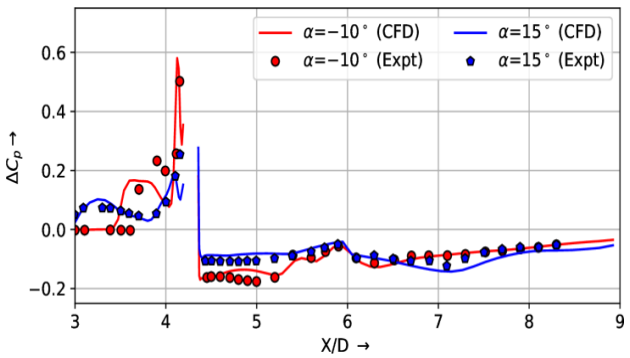

Figure 3: Comparison of pressure distribution over the validation model

Figure 3 depicts a comparison between the differential pressure coefficient along the top center-line obtained from the simulation and the corresponding experimental data. The results of the grid verification study are concisely presented in Table 1, with the "Exact" values derived through Richardson extrapolation between the medium and fine grids. The analysis reveals that the interaction significantly impairs the effectiveness of the jet, leading to a reduction of 35%. Moreover, the computed value of the jet effectiveness, 0.655, demonstrates excellent agreement with the values reported by James (2015), ranging from 0.64 to 0.66 depending on the turbulence model employed.

Table 1. Variation of the force coefficients with grid size

Grid size	ΔF	F_{jet}	E_{jet}
0.33×10^6	0.246	0.396	0.621
0.77×10^6	0.257	0.396	0.650
1.57×10^6	0.259	0.395	0.657
Exact (RE)	0.258	0.395	0.655
GCI (%)	0.329	0.027	0.416

C. Computational Domain and Grid

Typical computational domain sizes for the scale resolving simulations on flat plate configurations reported in literature for the jet in supersonic crossflow configurations ranged from about $100cm^3$ to $1000cm^3$. For the present axi-symmetric configuration, the computational domain size is over $8000cm^3$ making it infeasible to resolve the entire domain with an LES- like spatial resolution. Instead of resolving the entire domain with a uniformly fine grid, it is more practical to use a finer grid in the region of interest, i.e., around the injected jet plume and a RANS-like mesh everywhere else. Two meshing approaches were used to achieve this objective. In the first approach, an "overset" grid topology in which a uniformly refined, structured block is overlaid on a RANS mesh was employed. For such overset grids, the solver "cuts" the "background" grid, which in this case corresponds to the RANS mesh, using the boundaries of the overset block. A single layer of cells that overlap the overset boundaries is retained in the background grid for communicating flow information between the two grids through solution interpolation. In the present case, a core region around the injection that fully encompasses the injected jet plume was considered for grid refinement. A structured block consisting of about 12 million cells at a resolution of about 0.4mm was constructed in this region as shown in figure 4.

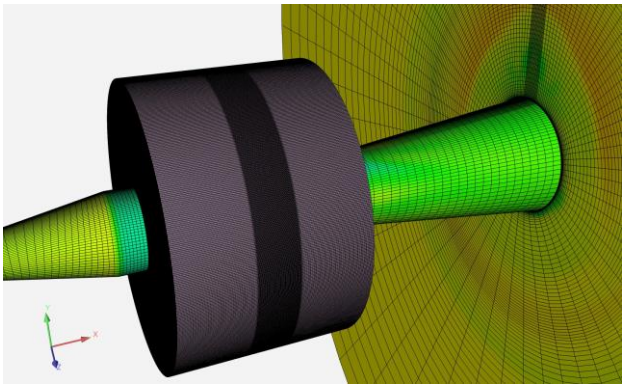

Figure 4: Computational grid with a refined overset block

The simulations were carried out using the Improved Delayed Detached Eddy Simulation (IDDES) model (Mikhail, et. al., 2008), and the unsteady solver with a time step size of $0.2\mu s$ which corresponds to a CFL number of 0.3 based on the finest grid spacing of 0.4mm. For studying the temporal fluctuations of the flow variables and for spectral analysis in the frequency domain, numerical probes were setup at several locations as shown in figure 5. A total of 72 probes were positioned in a regular grid pattern with 9 probes in the axial direction and 8 probes in the radial direction.

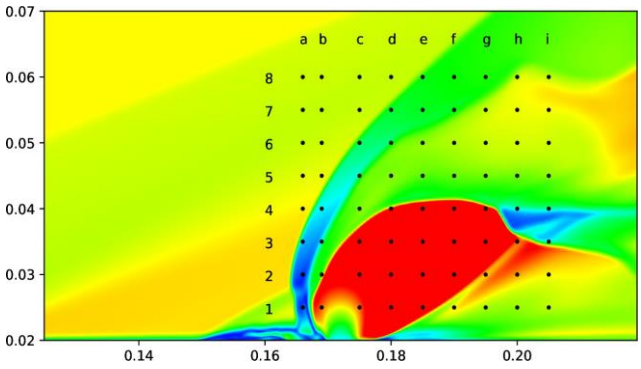

Figure 5: Probe locations for the DES

The second approach to generating the computational grid is the conventional technique which consists of building up the computational domain with edges and faces of the desired resolution. This approach results in fully structured blocks and avoids the cross-zone interpolation that is needed for the overset topology. Two such grids, consisting of about 8million and 12million cells were created with a

uniform core region with a spacing of 0.6mm and 0.4mm around the injection respectively. This core region is the LES zone and corresponds roughly to the structured overset block in terms of the axial and radial extents. In the azimuthal direction, uniform spacing was used up to an angle of 90° from the injection instead of all the way to the bottom as was done for the overset block. This was done to reduce the total cell count to a manageable level. From this core region, a low stretching factor (≈ 1.1) was used to gradually increase the mesh spacing to a RANS-like resolution towards the domain boundaries as shown in figure 6. These conformal grids were used to study the effect of a top-hat injection profile on the interaction force and the corresponding results are discussed in subsequent section.

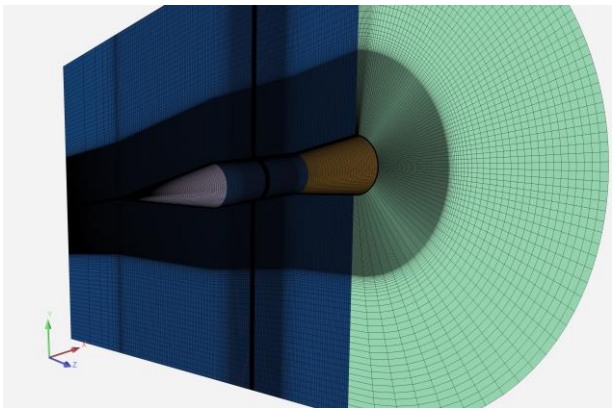

Figure 6: Computational grid with local clustering

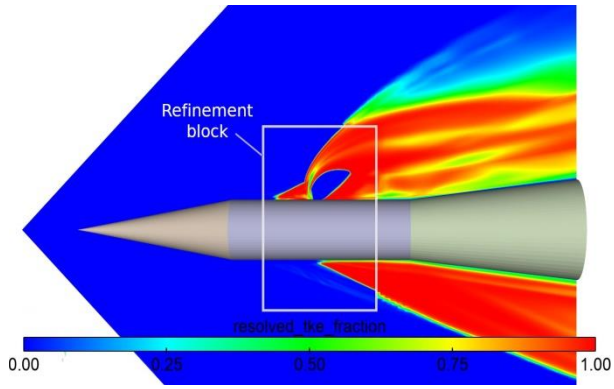

Figure 7: Resolved TKE fraction

3. RESULT ANALYSIS

A. Steady Injection

Contours of the resolved fraction of the turbulent kinetic energy are shown in figure 7. It is seen that most of the turbulent kinetic energy is resolved in the core region where the refined block is present. This indicates that the core block grid resolution is adequate for LES. Instantaneous ISO-surfaces of Q-criterion colored by Mach number are shown in figure 8. The generation of vortices ahead and around the injected jet, the wrapping of these vortical structures towards the bottom region and their breakdown into smaller vortices is clearly seen. The contours of Mach number at four instants separated by 50μs are shown in figure 9. The generation and downstream convection of the large-scale structures in the shear layer between the barrel shock and the bow shock can clearly be seen.

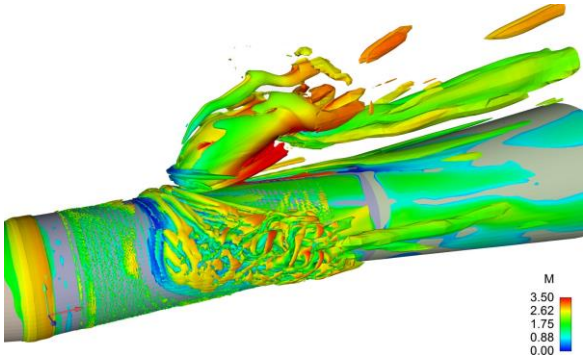

(a) Q-criterion = 10^8

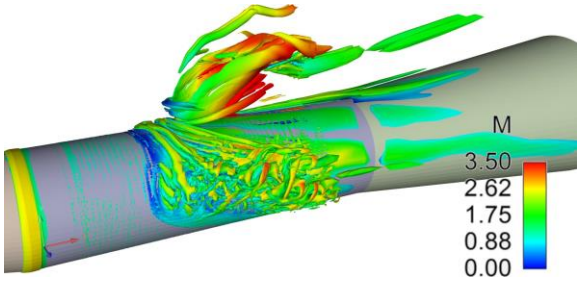

(b) Q-criterion = 10^9

Figure 8: ISO-surface of Q-criterion

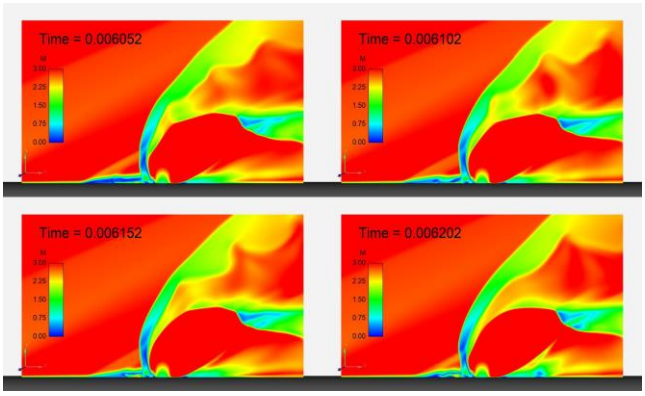

Figure 9: Contours of Mach number in symmetry plane at different instants

B. Spectral Analysis

The transient pressures and pressure spectra at probe locations corresponding to low, moderate and high temporal variations are shown in figures 10, 11 and 12 respectively. The temporal pressure fluctuations are large at the bow

shock (probe locations c6 and d7), at the barrel shock (d4) and in the region between the bow shock and the barrel shock (a1, a2 and b2). These large amplitude fluctuations indicate unsteadiness of these shock structures. Moderate fluctuations are seen for the probes in the upper right quadrant of Figure 5 which is the mixing region above the barrel shock and behind the bow shock as well as in the wake behind the injection. The lowest pressure fluctuations, which are negligible, are present inside the expanding injected jet. The pressure spectra all show a similar trend with most of the energy lying below a Strouhal number (based on jet diameter and free stream velocity) of about 0.3. This is consistent with the findings reported in literature (Warrick, et. al. 2018). The spectra of turbulent kinetic energy computed at the probe locations corresponding to the moderate and high fluctuations are shown in Figures 13a and 13b. These spectra also follow a trend similar to the pressure spectra with most of the energy contained in the lower Strouhal numbers (<0.3).

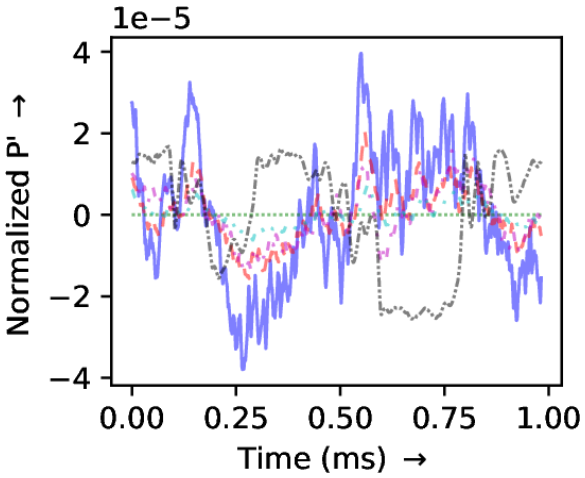

(a) Normalized pressure

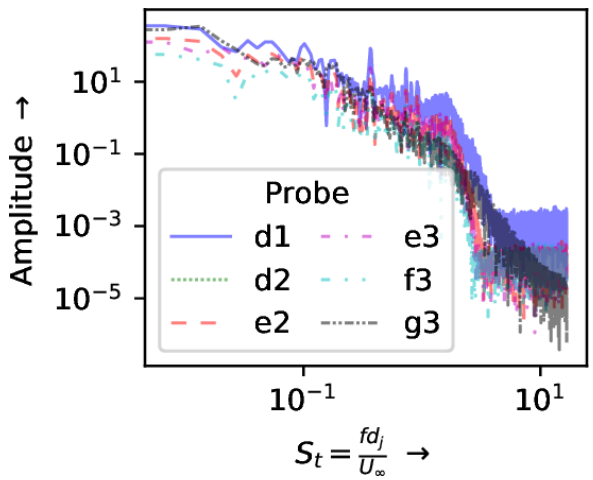

(b) Pressure spectrum

Figure 10: Transient pressure at locations of low fluctuations

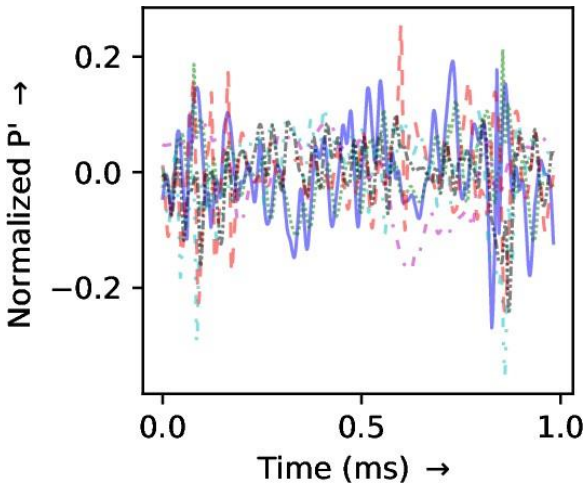

(a) Normalized pressure

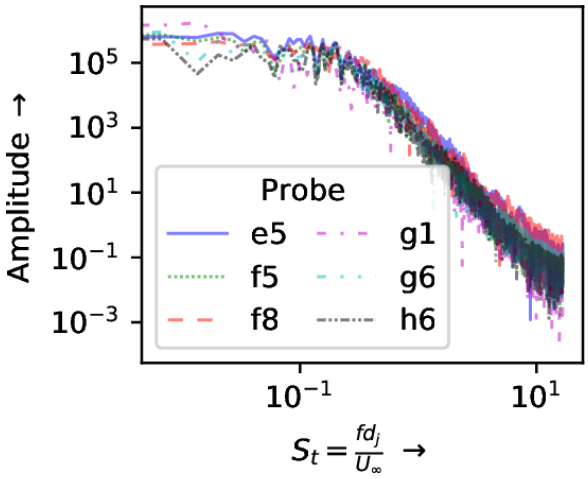

(b) Pressure spectrum

Figure 11: Transient pressure at locations of moderate fluctuations

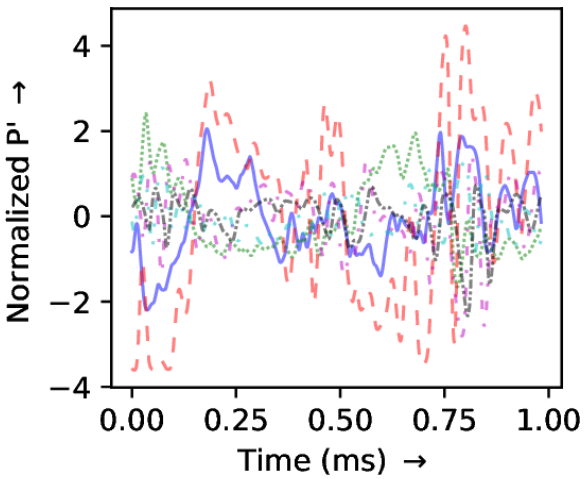

(a) Normalized pressure

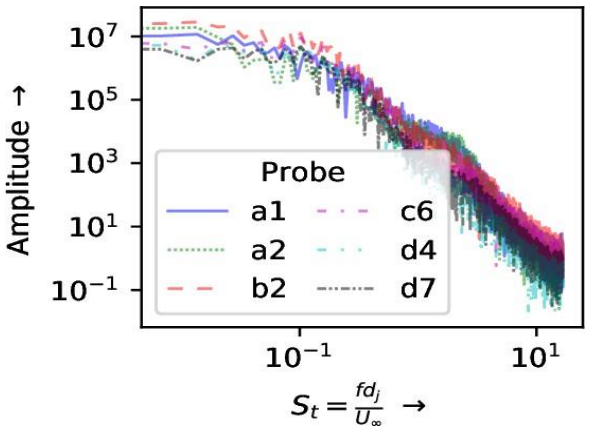

(b) Pressure spectrum

Figure 12: Transient pressure at locations of high fluctuations

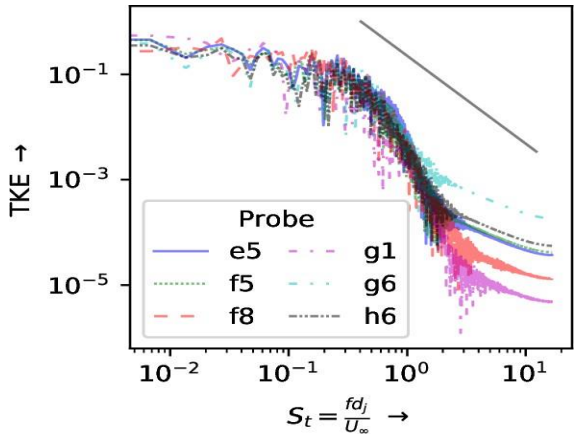

(a) Moderate fluctuations

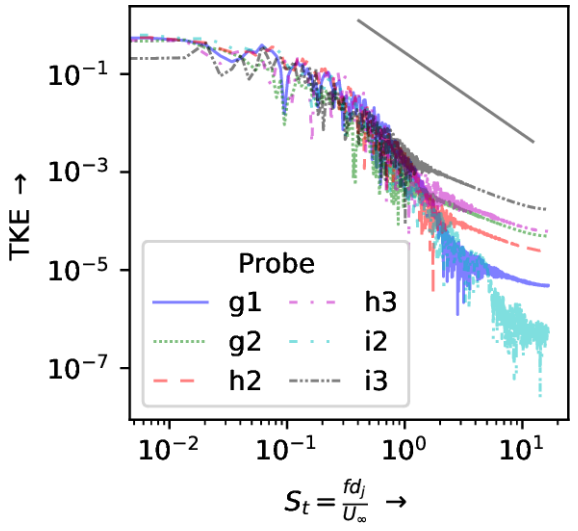

(b) High fluctuations

Figure 13: Spectral behavior of the turbulent kinetic energy

C. *Comparison of DES and RANS*

For comparison with RANS, simulations were carried out on the RANS mesh without the overset block to study the influence of turbulence models on the interaction force. For this purpose, the following models were used:

1. Inviscid simulation, by treating the fluid as non-viscous.
2. SST-$k-\omega$ model.
3. Realizable $k-\varepsilon$ model.
4. Reynolds stress model.

These RANS simulations were all run in the steady state mode. The convergence history of the normalized interaction force from these simulations is shown in figure 14. It is seen that the steady state value of the interaction force obtained from all the models is within 5% of the mean. While the DES on the RANS mesh failed to capture any unsteadiness in the interaction force, the simulation with the overset block has captured significant unsteadiness. The time-averaged value of the interaction force from this simulation is again within the same 5% band about the mean with the amplitude of the oscillations roughly corresponding to the band of variation among the various turbulence models.

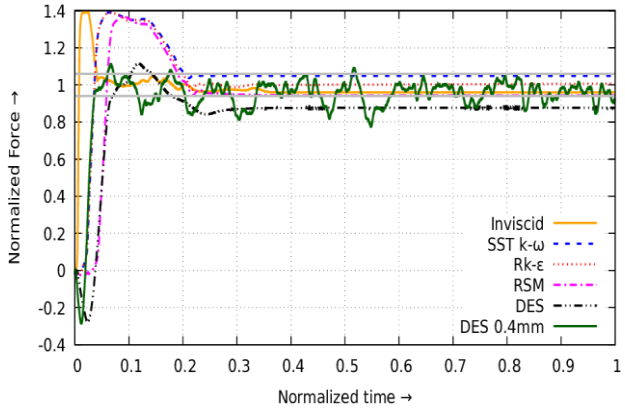

Figure 14: Convergence history of interaction force

D. *Top-Hat Injection Profile*

Another set of DES was carried out for a jet injection pulse with a top-hat injection profile. For this mode of injection, the simulation is started with the side jet off. At a predefined time instant, the side jet is abruptly switched on; injection is continued for a specified duration and is then withdrawn abruptly. Three models were used for these simulations:

1. Unsteady-RANS or URANS
2. Batten-Goldberg hybrid RANS/LES, also called Limited Numerical Scales (LNS)
3. Improved Delayed Detached Eddy Simulation (IDDES) model

For all these simulations, the conformal mesh shown in Figure 6 was used and the initial state of the flow corresponds to the steady free stream condition without an injected jet. A comparison of the variation of interaction force with non-dimensional time, for URANS and LNS on the two grids with core resolutions of 0.6mm and 0.4mm is shown in figure 15a.

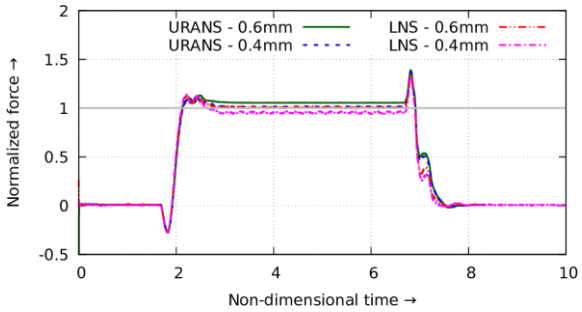

(a) Effect of grid resolution

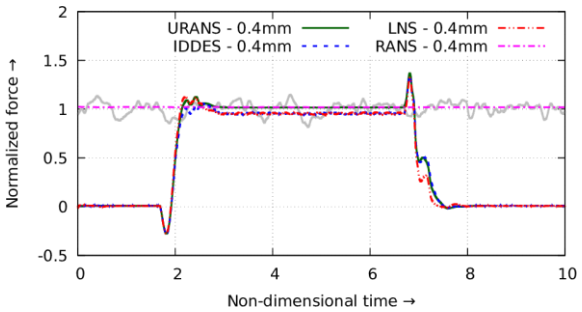

(b) URANS vs DES on the finer grid

Figure 15: Interaction force for a top-hat profile

The non-dimensional time, τ, in this figure is defined as the ratio of physical time to the domain flow-through time. The interaction force in these graphs was normalized using the mean value from all these simulations between $\tau = 4$ and $\tau = 6$ and this mean is shown as the grey horizontal line in the graph. It is seen that the statistically steady values of the LNS simulations are very close to the steady values of the URANS simulations. The standard deviation for these four simulations was about 2.3%.

An additional simulation using IDDES on the finer grid (0.4mm resolution) was run to see if the specific DES model had any effect on the interaction force. A comparison of the three unsteady simulations using URANS, LNS and IDDES along with a reference steady RANS simulation is shown in figure 15b. The results from the IDDES simulation on the overset grid discussed in earlier section corresponding to steady injection is also presented for reference as the grey curve in the figure. Here too, it is seen that all the simulations agree rather closely with each other, with a notable difference being the higher amplitude oscillations seen for the IDDES on the overset mesh.

9. CONCLUSIONS

Scale resolving simulations using hybrid RANS+LES were carried out for the interaction between an injected reaction control jet and a supersonic crossflow over an axi-symmetric body. The number of grid nodes and spatial resolutions used in these simulations were comparable to those reported in literature for similar flows. The DES results were compared with simulations based on RANS using different turbulent models. Spectral analysis was carried out using both time-series data collected at various locations of interest.

These simulations have enabled an assessment of the expected fluctuations of the interaction force about the statistical mean as predicted using plain RANS/URANS. It was seen that the mean force predicted from the scale resolving simulations was within the band of variability of the RANS simulations and varied by 5% about the mean value. The meshing approach used to resolve the LES part of the domain appears to have an effect on the amplitude of oscillations of the interaction structures. More detailed studies are required in this regard to be able to make definite recommendations regarding the superiority of any specific meshing approach.

Finally, it must me mentioned that the computational resources required for the scale resolving simulations in terms of CPU-hours and disk storage were about two orders of magnitude larger than the steady state RANS simulations even though only a relatively small region of the entire domain was resolved to LES levels. RANS models are better suited for exploratory studies involving large number of simulations with parameter variations for which the specific temporal evolution of the large-scale structures is not particularly important.

REFERENCES

Adela Ben-Yakar. (2000). Experimental investigation of mixing and ignition of transverse jets in supersonic crossflows. [Doctoral dissertation]. USA, Stanford University.

Adrian S. Pudsey, Russell R. Boyce, and Vincent Wheatley. (2013). Influence of Common Modeling Choices for High-Speed Transverse Jet-Interaction Simulations. *Journal of Propulsion and Power* 29.5, pp. 1076–1086. DOI: 10.2514/1.b34750.

André, T., Durant, A. and Fedioun. I. (2017). Numerical Study of Supersonic Boundary-Layer Transition due to Sonic Wall Injection. *AIAA Journal* 55.5, pp. 1530– 1547. DOI: 10.2514/1.j055164.

Antonino Ferrante, Georgios Matheou, and Paul E. Dimotakis. (2011). LES of an inclined sonic jet into a turbulent crossflow at Mach 3.6. *Journal of Turbulence* 12, N2. DOI: 10.1080/14685248.2010.522580.

Dean Dickmann and Frank Lu. (2006). Jet in Supersonic Crossflow on a Flat Plate. In: *25th AIAA Aerodynamic Measurement Technology and Ground Testing Conference*. American Institute of Aeronautics and Astronautics (AIAA), USA. DOI: 10.2514/6. 2006-3451.

James DeSpirito. (2015). Turbulence Model Effects on Cold-Gas Lateral Jet Interaction in a Supersonic Crossflow. *Journal of*

Spacecraft and Rockets 52.3, pp. 836–852. DOI: 10.2514/1.a32974.

John A. Boles, Jack R. Edwards, and Robert A. Bauerle. (2010). Large-Eddy/Reynolds-Averaged Navier-Stokes Simulations of Sonic Injection into Mach 2 Crossflow. *AIAA Journal* 48.7, pp. 1444–1456. DOI: 10.2514/1.J050066.

Julius Brandeis and Jacob Gill. (1996). Experimental investigation of side-jet steering for supersonic and hypersonic missiles *Journal of Spacecraft and Rockets* 33.3, pp. 346–352. DOI: 10.2514/3.26766.

Junya Watanabe et al. (2011). Numerical Study on Turbulent Structure of Transverse Jet into Supersonic Flow. *AIAA Journal* 49.9, pp. 2057–2067. DOI: 10.2514/ 1.j051067.

Krishnan Mahesh. (2013). The Interaction of Jets with Crossflow. *Annual Review of Fluid Mechanics* 45.1, pp. 379–407. DOI: 10.1146/annurev-fluid-120710-101115.

Mikhail L. Shur et al. (2008). A hybrid RANS-LES approach with delayed-DES and wall modeled LES capabilities. *International Journal of Heat and Fluid Flow* 29.6, pp. 1638–1649. DOI: 10.1016/j.ijheatfluidflow.2008.07.001.

Mitsura Kurita, Takumi Okada, and Yoshiaki Nakamura. (2001). The effects of attack angle on aerodynamic interaction due to side jet from a blunted body in a supersonic flow. *39th Aerospace Sciences Meeting and Exhibit*. American Institute of Aeronautics and Astronautics (AIAA). DOI: 10.2514/6.2001-261.

Patrick Roache. (2003). Error Bars for CFD. *41st Aerospace Sciences Meeting and Exhibit*. American Institute of Aeronautics and Astronautics. DOI: 10.2514/6.2003- 408.

Raj Kiran Grandhi and Arnab Roy. (2017). Effectiveness of a Reaction Control System jet in a Supersonic Crossflow. *Journal of Spacecraft and Rockets*. DOI: 10.2514/ 1.a33770.

Raj Kiran Grandhi and Arnab Roy. (2019a). Performance of Control Jets on Curved Bodies in Supersonic Cross Flows. *Journal of Spacecraft and Rockets*, pp. 1–12. DOI: 10.2514/1.a34314.

Raj Kiran Grandhi and Arnab Roy. (2019b). Performance of tandem control jets in supersonic cross flows. *Proceedings of the 16th Asian Congress of Fluid Mechanics*. Paper 251.

Raj Kiran Grandhi and Arnab Roy. (2021). Effect of Axial Location on the Performance of a Control Jet in a Supersonic Cross Flow. *Lecture Notes in Mechanical Engineering*. Springer Singapore, pp. 89–104. DOI: 10.1007/978-981-15-9601-8_7.

Raj Kiran Grandhi and Arnab Roy. (2023). Transient response of a reaction control jet injected into a supersonic cross flow. *Ninth Symposium on Applied Aerodynamics and Design of Aerospace Vehicles*. Paper 027.

Rana, Z. A., Thornber, B. and Drikakis. D. (2011). Transverse jet injection into a supersonic turbulent cross-flow. *Physics of Fluids* 23.4, p. 046103. DOI: 10.1063/ 1.3570692.

Ravichandra Srinivasan and Rodney Bowersox. (2005). Assessment of RANS and DES Turbulence Models for Supersonic Jet Interaction Flows. *43rd AIAA Aerospace Sciences Meeting and Exhibit*. American Institute of Aeronautics and Astronautics (AIAA). DOI: 10.2514/6.2005-499.

Rhea George et al. (2011). Flow-field analysis of SITVC in a contoured nozzle. *Fifth Symposium on Applied Aerodynamics and Design of Aerospace Vehicles*. Paper 006.

Sadatake Tomioka, Lance Jacobsen, and Joseph Schetz. (2000). Interaction between a super- sonic airstream and a sonic jet injected through a diamond-shaped orifice. *38th Aerospace Sciences Meeting and Exhibit*. American Institute of Aeronautics and Astronautics (AIAA). DOI: 10.2514/6.2000-88.

Soshi Kawai and Sanjiva K. Lele. (2010). Large-Eddy Simulation of Jet Mixing in Supersonic Crossflows. *AIAA Journal* 48.9, pp. 2063–2083. DOI: 10.2514/1. j050282.

Stahl, B., Esch, H. and Gülhan. A. (2008). Experimental investigation of side jet interaction with a supersonic cross flow. *Aerospace Science and Technology* 12.4, pp. 269–275. DOI: 10.1016/j.ast.2007.01.009.

Su-Hee Won et al. (2010). Numerical Investigation of Transverse Hydrogen Jet into Super- sonic Crossflow Using Detached-Eddy Simulation. *AIAA Journal* 48.6, pp. 1047–1058. DOI: 10.2514/1.41165.

Valerio Viti, Reece Neel, and Joseph A. Schetz. (2009). Detailed flow physics of the supersonic jet interaction flow field. *Physics of Fluids*, 21.4, p. 046101. DOI: 10.1063/ 1.3112736.

Xiaochuan Chai, Prahladh S. Iyer, and Krishnan Mahesh. (2015). Numerical study of high speed jets in crossflow. *Journal of Fluid Mechanics* 785, pp. 152–188. DOI: 10.1017/jfm.2015.612.

Warrick A. Miller et al. (2018). Transient interaction between a reaction control jet and a hypersonic crossflow. *Physics of Fluids* 30.4, p. 046102. DOI: 10.1063/ 1.5018877.